

Molecular Dynamics Simulation of Ratchet Motion in an Asymmetric Nanochannel

M. Chinappi,¹ E. De Angelis,¹ S. Melchionna,² C. M. Casciola,¹ S. Succi,³ and R. Piva¹

¹*Department of Mechanics and Aeronautics, University of Rome "La Sapienza", via Eudossiana 18, 00184 Rome, Italy*

²*INFM-SOFT, Department of Physics, University of Rome "La Sapienza", P.le A. Moro 2, 00185 Rome, Italy*

³*Istituto Applicazioni Calcolo, CNR, viale del Policlinico 137, 00161 Rome, Italy*

(Received 8 May 2006; published 6 October 2006)

The persistence of ratchet effects, i.e., nonzero mass flux under a zero-mean time-dependent drive, when many-body interactions are present, is studied via molecular dynamics (MD) simulations of a simple liquid flowing in an asymmetric nanopore. The results show that (i) ratchet effects persist under many-body density correlations induced by the forcing; (ii) two distinct linear responses (flux proportional to the drive amplitude) appear under strong loads. One regime has the same conductivity of linear response theory up to a forcing of about 10 kT, while the second displays a smaller conductivity, the difference in responses is due to geometric effects alone. (iii) Langevin simulations based on a naive mapping of the many-body equilibrium bulk diffusivity, D , onto the damping rate, γ are also found to yield two distinct linear responses. However, in both regimes, the flux is significantly smaller than the one of MD simulations.

DOI: 10.1103/PhysRevLett.97.144509

PACS numbers: 47.61.-k, 47.11.Mn, 47.56.+r, 66.90.+r

Recent progresses in the miniaturization of flow devices place a strategic value on theoretical and simulational techniques able to promote a deeper insight of the complex phenomena which control transport at nanoscopic scales. Nonequilibrium transport is of great relevance also in the biological context. Migration of water and ions across ion channels is a well-known example of finely tuned biological transport [1], whereas the conversion of chemical into mechanical energy in molecular pumps is prototypical of biological machines. In general, there is a great need to grasp the basic mechanism by which molecules can flow across nanoconfined geometries, where the large surface-volume ratios present a steep dissipative barrier to fluid motion. A fascinating phenomenon in this respect is the so-called ratchet motion [2], namely, the capability of nanofluids to exhibit a net mass transport under a zero-average dynamic load, or even the possibility to achieve negative particle mobility (net motion in the direction opposite to the drive) [3] and to rectify thermal fluctuations [4]. To date, ratchet phenomena have been studied mostly by means of one-body Langevin (or Fokker-Planck) descriptions [2,5], in which the many-body features of molecular motion are conveyed into an effective drag coefficient, representing the systematic interaction with the surrounding fluid, and a noise term, surrogating the collective motion of the molecules with a source of randomness [6]. The Langevin approach has been widely applied also to the study of realistic ion channels [7–9]. Conversely, previous work has shown the influence of cooperative motion on ratchet systems, most notably the observation of current reversal of Brownian hard rods [10], the rectifying capability of conical nanopores [11] and spontaneous ratchet motion in granular gas [12]. Assessing the robustness of ratchet phenomena towards many-body effects is thus of great interest, both as a conceptual issue in non-equilibrium statistical mechanics, as well as to develop practical investigation tools for applications in nanotech-

nology and biology. In this work, we take a step along this direction via nonequilibrium MD simulations of confined asymmetric nanoflows.

Our target system is a so-called entropic ratchet [13], a conical nanopore where the longitudinal motion is driven by an external field, while the transversal motion is dominated by a symmetry breaking in geometrical confinement. At variance with the original model of entropic trapping, which is known to exhibit negative relative resistance and rectification [13], our model system retains the essential features of many (biological) nanochannels, most notably spatial asymmetry [7]. We consider a truncated-cone channel of height $h = 8 \text{ \AA}$ and circular sections of radii $R_1 = 7.5 \text{ \AA}$, $R_2 = 12.5 \text{ \AA}$, i.e., a divergent channel toward the positive orientation of the z axis (see Fig. 1). The channel is embedded into a triperiodic box of size $L_x = L_y = 55 \text{ \AA}$ and $L_z = 40 \text{ \AA}$. The MD simulations refer to liquid Argon atoms, at a density 0.835 amu/\AA^3 , and temperature $\theta = 87.8 \text{ K}$. The atoms interact through a 6–12 Lennard-Jones potential, with the following param-

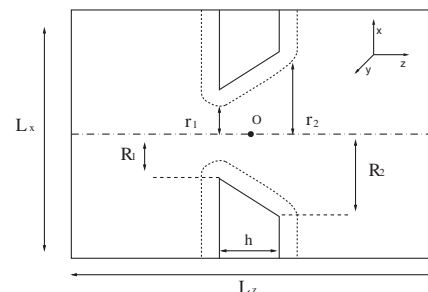


FIG. 1. Sketch of xz section of the simulation box at $y = 0$, (the origin of axes O is taken in the center of the channel). The solid line is the wall surface, the dashed one is the isosurface $[V_w(\mathbf{r}) = k_b\theta]$ of argon-wall potential. The effective radii of the pore (r_1 and r_2) are also indicated.

ters $\epsilon/k_b = 119.67$ K, with k_b the Boltzmann constant, and $\sigma = 3.405$ Å. Moreover, the atoms interact with the solid wall through a potential of the form $V_w(\mathbf{r}) = \int_{D_w} n_w f(|\mathbf{r} - \mathbf{r}_w|) d\mathbf{r}_w$, where D_w is the wall domain and $f(r)$ is the Lennard-Jones potential between a wall atom at the position \mathbf{r}_w and a liquid particle located at \mathbf{r} . In the above, $n_w = 0.033$ atoms/Å³ is the density of the wall atoms. The Argon-wall potential has the following parameters $\epsilon_w/k_b = 87.7$ K, $\sigma_w = 3.45$ Å. The Lennard-Jones parameters, used in previous computational studies [14], correspond to a CH₃ group in a hydrocarbon chain. In view of the soft nature of the liquid-wall interaction, the effective pore seen by the atoms [i.e., the isosurface $V_w(\mathbf{r}) = k_b\theta$] lies at radii $r_1 \simeq 5$ Å and $r_2 \simeq 10$ Å at the two channel mouths (see Fig. 1). The MD equations are advanced using the velocity Verlet scheme [15], with a time step 0.005 ps, the potentials are truncated at $r_{\text{cut}} = 12$ Å. The simulations have been performed using software package DLPROTEIN [16]. Coupling of the system to the heat bath is achieved via a Berendsen thermostat [17], with a characteristic time $\tau_b = 0.5$ ps. The choice for this thermostat, in lieu of other possible choices (e.g., Nosé-Hoover), was dictated by the need to minimize possible memory effects under periodic load. The overdamped Berendsen dynamics offers such possibility. However, on preliminary studies we have checked that the Berendsen and Nosé-Hoover dynamics produced similar responses. Results were found to be robust against changes in the coupling time 0.05 ps $< \tau_b < 1.5$ ps.

The instantaneous particles flux through the channel is computed by means of the expression

$$\phi(t) = \frac{1}{h} \sum_i' v_{zi}(t), \quad (1)$$

where v_{zi} is the z component of the velocity of the i th atom and the prime stands for summation over atoms in the channel ($-h/2 < z_i < h/2$) at time t . Alternatively, the flux can be interpreted as the time derivative of the collective variable (see Zhu *et al.* [18]) scoring ± 1 for each atom crossing the channel from left/right to right/left.

As a preliminary step, we compute the particle flux under a static external drive. The dynamic behavior under zero-average periodic forcing will be investigated later on. After an initial transient, a steady state is observed and an average mass flux, Φ , is computed. Figure 2 illustrates the flux Φ as a function of the forcing amplitude, A_s , parallel to z . The results for the truncated-cone geometry are shown, as well as those for the reference cases of two straight cylinders with height h and effective radii r_1 and r_2 , respectively. Several remarks are in order.

First, we observe a distinct symmetry breaking between positive (rightward) versus negative (leftward) forcing. This lack of symmetry reflects the intuitive notion that atoms flow more easily along the convergent direction

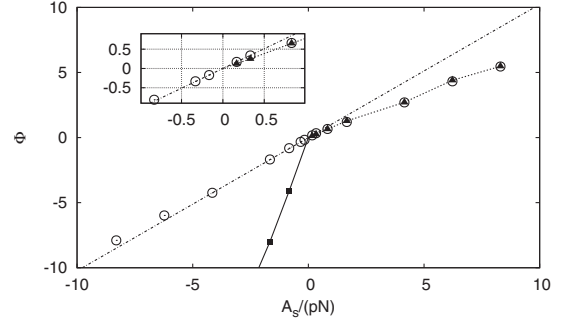


FIG. 2. Particle flux (atoms/ps) vs the static forcing amplitude A_s . Black triangles $1 \rightarrow 1$ geometry, squares $2 \rightarrow 2$ geometry, circles conical pore geometry, dot-dashed line linear response prediction.

(conventionally denoted as $2 \rightarrow 1$) than along the divergent one (denoted as $1 \rightarrow 2$). A closer inspection reveals however a number of subtleties behind this simple and intuitive picture. To better appreciate this point, it is instructive to compare the results with those of two straight cylinders, with effective radii r_1 ($1 \rightarrow 1$ for notational convenience), and r_2 ($2 \rightarrow 2$), respectively.

The first observation is that at sufficiently large amplitudes, i.e., $A_s \gtrsim 0.5$ pN, the flux $\Phi_{1 \rightarrow 2}$ virtually coincides with $\Phi_{1 \rightarrow 1}$. In other words, the atoms do not “see” the additional space offered by the expanding cross section along the flight direction. This can be explained as follows. Let us define an advective flight time $\tau_a = h/u$ (i.e., the time needed by a particle to cross the pore) where u is a characteristic velocity of a particle in the channel. This velocity can be estimated as $u = \Phi_{1 \rightarrow 2} / \rho_n \pi r_1^2$, ρ_n being the number of particles per Å³. A diffusive time can also be defined as $\tau_d \simeq \bar{r}^2 / 2D$, $\bar{r} = (r_1 + r_2) / 2$ (i.e., the time needed by a particle near the axis to diffuse transversely in the pore), where D is the bulk diffusion coefficient of argon. The two time scales match approximately at $\Phi \simeq 0.1$. For $\tau_a \ll \tau_d$ the particles do not have sufficient time to explore the full space offered by the truncated-conical geometry, so that $\Phi_{1 \rightarrow 2} \simeq \Phi_{1 \rightarrow 1}$. Conversely, in the low-forcing regime, atoms have time to diffuse across the main flow, and, consequently, they visit all the space offered by the conical geometry. As a result, no significant difference is expected between leftward and rightward motion. Indeed, a close up of Fig. 2 reveals that for $A_s \lesssim 0.5$ pN, $\Phi_{1 \rightarrow 2}$ and $\Phi_{2 \rightarrow 1}$ lie on the same straight line. The slope of this line can be predicted as follows. Let us consider an ensemble of systems at thermodynamic equilibrium at time $t = 0$, perturbed by the static external force A_s at $t > 0$. At low forcing, the ensemble average of instantaneous flux $\langle \phi(t) \rangle$ is given by linear response theory [19] as

$$\langle \phi(t) \rangle = \frac{A_s}{k_b T} \int_0^t \left\langle \phi(s) \sum_i v_{zi}(0) \right\rangle_{\text{eq}} ds, \quad (2)$$

where the sum runs over all atoms and $\langle \rangle_{\text{eq}}$ indicates aver-

age at equilibrium. The mean flux in stationary regime Φ , as obtained in the limit $t \rightarrow \infty$, yields $\Phi/A_s \approx 1.02$ (atoms/ps)/pN. This value is in excellent agreement with the simulation data (see Fig. 2, inset).

The case of right-to-left forcing is quite different. It is observed that the flux for the straight cylinder $\Phi_{2 \rightarrow 2}$ is considerably larger than for the truncated cone, namely, $\Phi_{2 \rightarrow 1} \approx 0.25\Phi_{2 \rightarrow 2}$, i.e., molecular motion along the convergent direction experiences a strong penalty due to the decreasing cross section. For the truncated-cone geometry, as already pointed out, at low amplitudes, the picture is just the same as for left-to-right forcing: the value is predicted by linear response theory. The linear prediction continues to hold also at very high amplitudes (i.e., $A_s L_z \gg k_b \theta$). Albeit surprising, this is nonetheless in line with previous findings from simulations of water in cylindrical pores of ≈ 10 Å size [18].

The emerging picture of the stationary process is quite neat. At low forcing, the flow obeys linear response theory and does not perceive the broken symmetry between the two directions. The onset of nonlinear effects associates with the “emergence” of the geometrical asymmetry, marked by the condition that the flight time τ_a along the channel be smaller than the diffusive time τ_d across it. Under such conditions the molecular flow is unable to visit the annular region offered by the expanding cross section. As a result, the net flux is the same as in a straight cylinder of radius r_1 . It is remarkable that at high forcing the $\Phi_{1 \rightarrow 2}$ response remains quasilinear, although with a slope very different from the value predicted by linear response theory. The robustness of the quasilinear regime suggests that the conical pore might serve as nanorectifier, whose response can be predicted by simple geometrical considerations for a wide range of external drives. This microscopic picture is confirmed by Fig. 3, in which the density profiles for equilibrium and steady-state configurations are shown. For $2 \rightarrow 1$ forcing, the data exhibit a rather uniform density

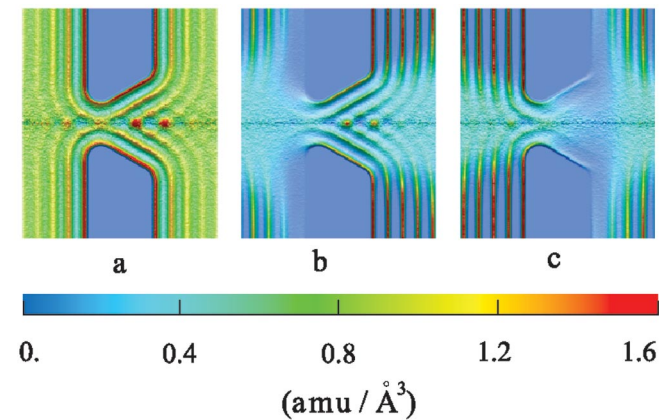


FIG. 3 (color). Density profiles on a symmetry plane: equilibrium (a), static forcing, $A_s = -4.15$ pN (b) and $A_s = 4.15$ pN (c).

inside the channel and a substantial layering, reminiscent of the unperturbed one, both inside and outside the pore region. Conversely, for $1 \rightarrow 2$ forcing, the profile exhibits a field-induced depletion of the expanding annular region and the absence of layering inside the pore region.

For the sake of comparison, we have also performed Langevin simulations with systematic drag, γ , and random forcing, ξ , tuned on the bulk value of the diffusion coefficient, D , computed from equilibrium MD simulations, that is $\gamma = kT/mD$ and $\langle \xi(t)\xi(t') \rangle = 2\gamma^2 D \delta(t' - t)$. These results also show a linear dependence of the mass flux on the forcing amplitude, although with significantly different slopes as compared to the MD case. More specifically, the Langevin mass flux is found to be about 5 and 8 times smaller than the MD one, in the two regimes corresponding to convergent and divergent directions, respectively. The discrepancy is likely due to the neglect of many-body interactions and related memory effects, inherent to the single-particle Langevin dynamics. An effective way to include concerted atomic flow within the channel would be to replace the friction term $-\gamma\mathbf{v}$ with $-\gamma(\mathbf{v} - \mathbf{u})$, \mathbf{u} being the macroscopic velocity field. However, the latter quantity is clearly not available in advance in the Langevin framework. The observed discrepancy thus provides a clear indication that the bulk diffusivity alone fails to capture the full picture behind the mapping of many-body interactions

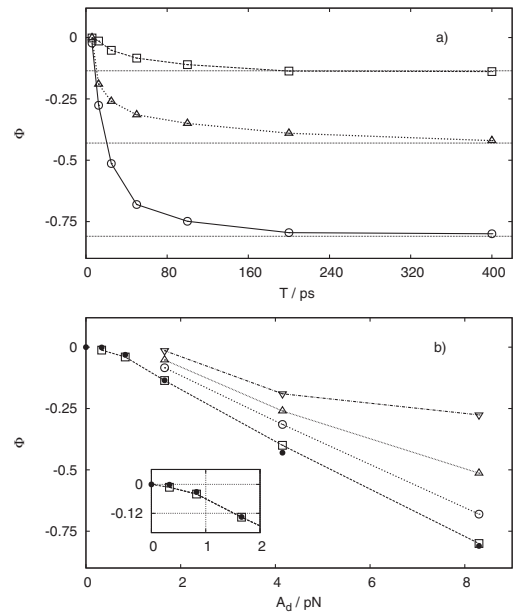


FIG. 4. (a) Particle flux Φ (atoms/ps) as function of the period T [Eq. (3)] at different amplitudes A_d . Squares $A_d = 1.66$ pN, triangles $A_d = 4.15$ pN, circles $A_d = 8.3$ pN. The three horizontal lines are the adiabatic plateaux obtained by numerical integration of (4). (b) Φ as a function of the dynamic forcing amplitude A_d for different periods T . Squares $T = 200$ ps, circles $T = 50$ ps, upper triangles $T = 25$ ps, lower triangles $T = 12.5$ ps. Filled circles: adiabatic values.

in a confined nanofluid, into an effective single-body Langevin representation.

Next, we explore the effects of dynamic forcing. In particular, we focus our attention on genuine ratchet effects, i.e., the onset of nonzero net particle flux in the face of zero-average time-dependent forcing, varying in time according to the following sinusoidal law

$$\mathbf{F}(t) = A_d \sin\left(\frac{2\pi t}{T}\right) \hat{\mathbf{z}}, \quad (3)$$

$\hat{\mathbf{z}}$ being the z -axis unit vector. In Fig. 4(a) we show the net flux Φ as a function of the period T for different values of amplitude A_d . It proves expedient to define as the internal time scale τ as the time needed by the system, initially at equilibrium, to reach the stationary regime under the effect of a static drive. At low forcing, the ensemble average of $\phi(t)$ is given by linear response theory—Eq. (2)—and τ can be roughly estimated from the behavior of $\langle\phi(t)\rangle$. In our case, $\tau \approx 10$ ps. For $T \lesssim \tau$ the flux vanishes; in line with the basic intuition that at high-frequency forcing there is no time for the system to absorb systematic momentum. By increasing the period T , we observe that the net flux becomes more and more negative, until, for $T \gg \tau$, saturation is reached. The negative sign is easily explained as follows. Since the static dependence $\Phi = \Phi(A_s)$, has broken symmetry $\Phi_{1 \rightarrow 2}(A_s) < -\Phi_{2 \rightarrow 1}(-A_s)$, $A_s > 0$, the net flux over a period T is negative because the positive flux driven in the first (direct) half-cycle is smaller than the negative flux in the second (reverse) half-cycle. The saturation is explained by noting that, for $T \gg \tau$, the system has enough time to adiabatically adjust to the instantaneous forcing. Thus, the flux can be estimated as

$$\Phi_{\text{ad}} \equiv \frac{1}{T} \int_0^T \Phi(F_z(t)) dt, \quad (4)$$

where $F_z(t)$ is the z component of $\mathbf{F}(t)$. For the instantaneous time-dependent flux $\Phi(F_z(t))$, we have assumed the mean flux under a static drive $\Phi(A_s)$, given in Fig. 2. The values of Φ_{ad} for different A_d has been numerically calculated starting from the data for static drive and found to be in good agreement with time-dependent forcing simulation [horizontal lines in Fig. 4(a)]. The dependence of the driven flux on the forcing amplitude A_d is shown in Fig. 4. From the figure it is observed that at vanishing values of A_d , the flux approaches zero along a bell-shaped curve [2]. Let us note that the values of Φ are bounded from below by the adiabatic limit Φ_{ad} [black circles in Fig. 4(b)].

Summarizing, we have shown that many-body atomistic simulations of nanoscopic flows in confined geometries with broken spatial symmetry do support evidence of ratchet effects. In line with previous findings, the intensity of these ratchet effects is found to grow with increasing

amplitude and decreasing frequency of the external drive [2]. However, at variance with one-body scenarios, (i) ratchet effects persist in the presence of significant layering effects of the density profile, (ii) the mass flux is consistently larger than the one predicted by a corresponding Langevin equation. This indicates that while the standard Langevin picture does capture the qualitative features of ratchet motion (linear response in both weak and strong-drive regimes), a quantitative prediction of the mass-flux requires a more sophisticated mapping entailing the presence of a comoving solvent. Clearly, this level of information is not available in advance in a simple single-body picture. The onset of ratchet motion is found to associate closely with the condition that the molecular flight time along the channel be smaller than the diffusive time across it and the flux is upper bounded by its adiabatic value.

-
- [1] B. Hille, *Ionic Channels of Excitable Membranes* (Sinauer, Sunderland, 1992), 2nd ed.
 - [2] P. Reimann, Phys. Rep. **361**, 57 (2002).
 - [3] A. Ros, R. Eichhorn, J. Regtmeier, T.T. Duong, P. Reimann, and D. Anselmetti, Nature (London) **436**, 928 (2005).
 - [4] P. Meurs, C. Van den Broeck, and A. Garcia, Phys. Rev. E **70**, 051109 (2004).
 - [5] P. Hanggi and P. Reimann, Appl. Phys. A **75**, 169 (2002).
 - [6] H. Risken, *The Fokker-Planck Equation* (Springer-Verlag, Berlin, 1989), 2nd ed.
 - [7] I. Kosztin and K. Schulten, Phys. Rev. Lett. **93**, 238102 (2004).
 - [8] W. Im and B. Roux, J. Mol. Biol. **322**, 851 (2002).
 - [9] J. Piasecki, R. J. Allen, and J. P. Hansen, Phys. Rev. E **70**, 021105 (2004).
 - [10] I. Derényi and T. Vicsek, Phys. Rev. Lett. **75**, 374 (1995).
 - [11] Z. Siwy, I. D. Kosinska, A. Fulinski, and C. R. Martin, Phys. Rev. Lett. **94**, 048102 (2005).
 - [12] D. van der Meer, P. Reimann, K. van der Weele, and D. Lohse, Phys. Rev. Lett. **92**, 184301 (2004).
 - [13] G. A. Cecchi and M. O. Magnasco, Phys. Rev. Lett. **76**, 1968 (1996).
 - [14] R. J. Allen, J.-P. Hansen, and S. Melchionna, J. Chem. Phys. **119**, 3905 (2003).
 - [15] M. P. Allen and D. J. Tildesley, *Computer Simulations of Liquids* (Clarendon, Oxford, 1987).
 - [16] S. Melchionna and S. Cozzini, *The DLPROTEIN User Manual* (University of Rome, “La Sapienza”, 2001).
 - [17] H. J. C. Berendsen, J. P. M. Postma, W. F. van Gunsteren, A. Di Nola, and J. R. Haak, J. Chem. Phys. **81**, 3684 (1984).
 - [18] F. Zhu, E. Tajkhorshid, and K. Schulten, Phys. Rev. Lett. **93**, 224501 (2004).
 - [19] D. J. Evans and G. P. Morris, *Statistical Mechanics of Nonequilibrium Liquids* (Academic, New York, 1990).